ACS OMEGA

http://pubs.acs.org/journal/acsodf

Article

Characterization and Application of a Synthesized Novel Poly(chlorobis(1,10-phenanthroline)resorcinolcobalt(II) chloride)-Modified Glassy Carbon Electrode for Selective Voltammetric Determination of Cefadroxil in Pharmaceutical Formulations, Human Urine, and Blood Serum Samples

Adane Kassa, Amare Benor, Getinet Tamiru Tigineh, and Atakilt Abebe*

Cite This: *ACS Omega* 2023, 8, 15181−15192

Read Online

ACCESS | Metrics & More | Article Recommendations | Supporting Information

ABSTRACT: Cefadroxil belongs to the β-lactam antibiotics, mainly used for the treatment of various bacterial infections, caused by Gram-positive and Gram-negative bacteria. However, it is also encountering serious bacterial resistance, necessitating continuous monitoring of its level in pharmaceutical and biological samples. This study presents a selective, accurate, and precise square-wave voltammetric method based on a novel poly(chlorobis(1,10-phenanthroline)resorcinolcobalt(II)chloride)-modified glassy carbon electrode (poly(CP_2RCoC)/GCE) for determination of cefadroxil (CDL). UV−vis spectroscopy, FT-IR spectroscopy, metal and halide estimation, CHN elemental analysis, and electrolytic conductivity measurement results confirmed the synthesis of the title complex modifier. Electrode characterization results revealed modification of the surface of the electrode by an electroactive and a conductive polymer film (poly(CP_2RCoC)/GCE), leading to an improved effective electrode surface area. In contrast to the bare electrode, the appearance of an irreversible oxidative peak at a much reduced potential with a 7-fold current enhancement at poly(CP_2RCoC)/GCE showed the catalytic effect of the modifier toward oxidation of CDL. The square-wave voltammetric current response of poly(CP_2RCoC)/GCE showed a linear dependence on the concentration of CDL in the range of 1×10^{-7}−3.0×10^{-4} M with a detection limit of 4.3×10^{-9}. The CDL level in the selected two tablet brands was in the range of 97.25−100.00% of their labeled values. The spike recovery results in tablet, human blood serum, and urine samples were 98.85−101.30, 99.20−100.39, and 98.10−99.99%, respectively. Interference recovery results with a less than 4.74% error, lower LoD, and wider dynamic range than the previously reported methods validated the potential applicability of the present method with excellent accuracy and sensitivity based on the novel mixed-ligand complex-modified GCE (poly(CP_2RCoC)/GCE) for determination of CDL in various real samples with a complex matrix.

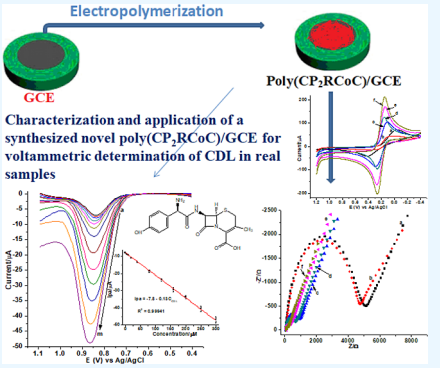

1. INTRODUCTION

The improper use of antibiotics results in environmental contamination, sensitivity, and resistance to broad-spectrum antibacterial drugs, which have detrimental impacts on both health and the economy.[1−3] In this respect, cephalosporins are among the most common drugs that have developed bacterial resistance.[2,4,5] Cefadroxil (6*R*,7*R*)-7-[[(2*R*)-2-amino-2-(4-hydroxyphenyl)acetyl]amino]-3-methyl-8-oxo-5-thia-1-azabicyclo[4.2.0]oct-2-ene-2-carboxylic acid) (CDL) (Scheme SM1) is an antibiotic drug which belongs to the cephalosporin class of the β-lactam family. It is a broad-spectrum, semisynthetic antibiotic. Gram-positive (*Streptococcus pneumoniae*, *Staphylococcus aureus*, and *Streptococcus pyogenes*) and Gram-negative (*Escherichia coli*) bacterial infections are treated with it.[1,6,7] However, it has common side effects like nausea, vomiting, diarrhea, joint pain, feeling agitated or hyperactive, an unpleasant taste, a skin rash, and vaginal itching.[1,2] Thus, monitoring the level of CDL in pharmaceutical formulations, biological, and other samples has been the task of the concerned bodies. For this purpose, spectrophotometry,[1,8] chromatography,[9,10] and LC-MS/MS[11] have been among the common techniques used and reported for the determination of CDL in different real samples. However, these techniques need large amounts of organic solvents, expensive instrumentation, and long analysis time, and they are non-eco-friendly.[12−15] In this regard, electrochemical methods includ-

Received: January 10, 2023
Accepted: April 6, 2023
Published: April 18, 2023

Scheme 1. Two-Step Synthesis of the CP_2RCoC Complex

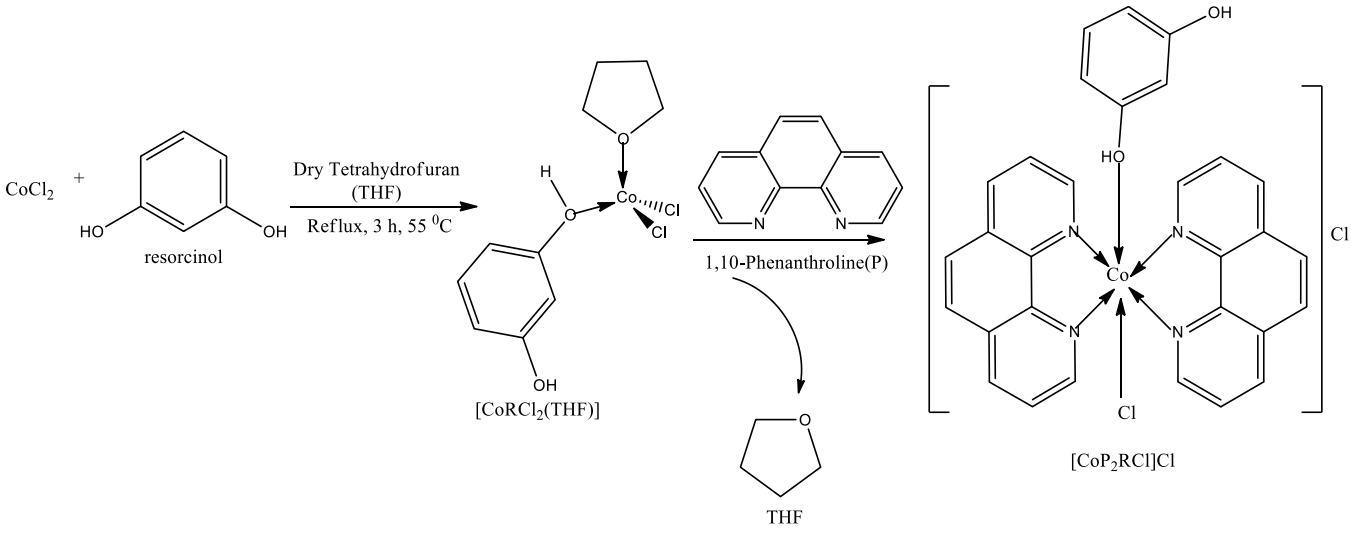

ing voltammetry are accurate, reproducible, fast, environmentally friendly, and often selective methods.[12−15] Developing a rapid, selective, sensitive, and stable method for the detection of CDL at its trace level in different matrices is crucial.

Transition-metal complexes have many unique proprieties such as highly accessible surface area, high chemical stability, and excellent electrocatalytic activity. Therefore, they have been widely applied in the fabrication of electrochemical sensors.[13,18] Researchers in the field of coordination chemistry have been drawn toward 1,10-phenanthroline (phen) because it interacts with metal ions via the nitrogen atom it contains, favoring the formation of metal complexes.[16,17] Similarly, resorcinol (1,3-dihydroxybenzene) is ascribed as one of the azo dyes which readily form stable complexes with most of the transition-metal ions.[19] Selective deprotonation of resorcinol (reso) achieved by mixing equimolar with NaOH monitors the site of complexation, leading to the formation of complexes.[20,21]

Modification of the surface of a working electrode usually improves its electrochemical performance by improving its compatibility, electron conductivity, mechanical properties, surface area, and control of the physicochemical nature of the electrode/solution interface.[18,22] Modifying materials are deposited at the electrode surface either by potentiodynamic electropolymerization,[15] potentiostatic electropolymerization,[7,13,18,23] or simply casting techniques.[24]

However, only a few studies have been reported on the electrochemical determination of CDL in different real samples using modified electrodes like carbon nanotube/Au nanoparticle-modified GCE,[25] nano-Ag-APMEs,[26] and poly(alizarin)/GCE.[7] Most of these reported methods require the use of expensive modifiers like Au nanoparticles with complex preparation procedures. Therefore, techniques combining inexpensive, nontoxic materials and straightforward procedures are needed to detect and identify medicines like CDL in various samples. From this angle, we present the low-cost and straightforward synthesis of a novel modifier. As a result, sensors made from these materials would also be affordable. The produced modifier, chlorobis(1,10-phenanthroline)resorcinolcobalt(II) chloride, is a mononuclear mixed-ligand Co(II) complex. Its characterization and sensor application are for the electrochemical assessment of CDL in tablet formulations, human blood serum, and urine samples.

2. MATERIALS AND METHODS

2.1. Chemicals and Apparatus. Cefadroxil monohydrate (≥99.0%, Sigma-Aldrich), silver nitrate (≥99.0%, Sigma-Aldrich), and 1,10-phenanthroline (≥99.7%, Sigma-Aldrich); potassium hexacyano ferrate (98.0%, BDH Laboratories Supplies, England), $CoCl_2{\cdot}6H_2O$ (99.0%, BDH laboratories supplies, England), and resorcinol (≥99.0%, BDH laboratories supplies, England); potassium chloride (99.5%, Blulux laboratories (p) Ltd), sodium monohydrogen phosphate, and sodium dihydrogen phosphate (≥98%, Blulux laboratories (p) Ltd); tetrahydrofuran (Anhui Royal Chemical Co., Ltd.), ethyl acetate (Loba Chemie), hydrochloric acid (37%, Fisher Scientific), nitric acid (70%, Fisher Scientific), and sodium hydroxide (Extra pure, Lab Tech Chemicals), all of analytical grade, were used without further purification.

A CHI 760E potentiostat (Austin, Texas, USA), pH meter (AD8000, Romania), refrigerator (Lec refrigeration PLC, England), deionizer (Evoqua water technologies), centrifuge (1020D, Centurion scientific LTD, UK), electronic balance (Nimbus, ADAM equipment, USA), portable pH/conductivity/TDS meter (Bante901P), UV−vis spectrophotometer (Cary 60, Agilent Technologies), FT-IR spectrophotometer (PerkinElmer, BX), ICP-OES spectrometer (PerkinElmer, Optima 7300V HF Version), and melting point apparatus (Stuart SMP30) were among the apparatuses used.

2.2. Electrochemical Measurement. A conventional three-electrode system with a bare GCE or poly-(CP_2RCoC)/GCE as a working electrode, Ag/AgCl (3.0 M KCl) as a reference electrode, and Pt coil as a counter electrode was used to perform electrochemical measurements. Electrochemical impedance spectroscopy (EIS) and cyclic voltammetry (CV) techniques were used to characterize poly(CP_2RCoC)/GCE and/or investigate the electrochemical behavior of CDL at the surface of poly(CP_2RCoC). Square-wave voltammetry (SWV) was employed for the quantitative determination of CDL in human blood serum, urine, and two brands of tablet samples.

2.3. Procedure. *2.3.1. Syntheses of the Metal Complex.* Chlorobis(1,10-phenanthroline)resorcinolcobalt(II) chloride

https://doi.org/10.1021/acsomega.3c00170
ACS Omega 2023, 8, 15181−15192

([CoP_2RCl]Cl) was prepared by a two-step reaction (Scheme 1). A blue-colored solution of $CoCl_2$ in dry tetrahydrofuran (THF) (0.36 g, 2.77 mmol, 40 mL) was mixed with a solution of reso in the same solvent (0.305 g, 2.77 mmol, 40 mL) and refluxed at 55 °C for 2 h while magnetically stirring in an oil bath. A bluish-green homogeneous solution was obtained, the solvent was removed under vacuum, and a dark-green mass was obtained. It was recrystallized from cold acetone, and a dark-green powder of the precursor complex ([$CoRCl_2$(THF)]) (C_2RTCo) was collected (yield: 0.833 g, 96.3%).

A solution of phen (0.348 g, 1.93 mmol) in 30 mL of THF was added from a dropping funnel to a blue−green solution of the magnetically stirred precursor complex ([$CoRCl_2$(THF)]) (0.60 g, 1.93 mmol) in 30 mL of THF at room temperature, and precipitate formation began right away. As the reaction came to a conclusion, the solution's blue−green color gradually turned lighter green and colorless at the end. The stirring continued for 1 h. The mixture was left to stand for the entire night. Then, the mixture was filtered using Whatman filter paper. The powder obtained was rinsed three times with 5 mL of methanol each. The powder was dried in open air. A brick-red powder of the target complex (CP_2RCoC) was collected (yield: 1.07 g, 93%).

2.3.2. Complex Characterization Procedures. The electrolytic conductance of synthesized complexes (C_2RTCo and CP_2RCoC) was measured at room temperature using a Bante901P portable pH/conductivity/TDS meter with a 1×10^{-4} M solution of each compound in deionized water. Using a Cary 60 UV−vis spectrophotometer, UV−vis spectra of a 1.0 mM solution of ligands, salt, and complexes in ethanol were recorded in the wavelength range of 200−800 nm. IR spectra were recorded using a BX spectrophotometer and roughly 200 mg of KBr as a matrix for 1 mg of each sample in the 4000−400 cm^{-1} range. ICP-OES was used to determine the cobalt content in each complex; in a 50 mL conical flask, 20 mg of each complex was combined with 5 mL of concentrated nitric acid and 5 mL of hydrochloric acid and gently heated until a few drops remained. This process was done three times more until the complex's organic portion was gone. The residue was then reconstituted in a 100 mL volumetric flask and diluted with deionized water until it reached the desired concentration. Ionizable chloride content was determined gravimetrically using the AgCl precipitate obtained from the mixture of 20 mg of the complex sample in 30 mL of distilled water with excess $AgNO_3$ solution. The cruddy white precipitate was then filtered and dried at 110 °C in an oven, from which the amount of chloride was estimated using the weight difference. The melting points of the compounds were determined by using the Stuart SMP30 melting point equipment.

2.3.3. Fabrication of the Poly(CP_2RCoC)-Modified GCE. A mirror-finished polished GCE was immersed in a 0.1 M phosphate buffer solution (PBS) of pH 7.0 containing 1.0 mM CP_2RCoC and scanned between an optimized potential window (−0.8 & +1.8 V) for 20 cycles at a scan rate of 100 mV s^{-1}. The poly(CP_2RCoC)/GCE was then rinsed with deionized water to remove the physically adsorbed monomer from the electrode surface. Subsequently, the modified electrode was stabilized in 0.5 M H_2SO_4 by scanning between −0.8 and +0.8 V until a stable CV was obtained. The poly(CP_2RCoC)/GCE was dried in open air and used for further experiments. The same procedure was followed for the preparation of the GCE modified with poly(phen), poly(reso), poly(C_2RTCo), and electrodeposited Co(0) from a solution of 1.0 mM of each monomer in pH 7.0 PBS.

2.3.4. Preparation of Standard CDL Solutions. A 5.0 mM stock solution of standard CDL in deionized water was prepared by adding an accurately weighed 182.7 mg of monohydrated CDL in a 100 mL volumetric flask. Working CDL standard solutions of CDL were prepared in PBS of the appropriate pH from the stock solution by serial dilution.

2.3.5. Preparation of Analyzed Real Samples. 2.3.5.1. Tablet Sample. Five randomly selected tablets from each of the two studied tablet brands of CDL [MeDIndian (Drox), India, and Medipol Pharmaceutical India Pvt. Ltd. (Cefacef), India] labeled as 500 mg of CDL/tablet with an average mass/tablet of 572.1 and 565.6 mg, respectively, were ground and homogenized using a mortar and pestle. A stock solution of the tablet sample with nominal (2.0 mM) for each tablet brand of CDL was prepared by transferring a mass of tablet powder equivalent to 76.28 mg of CDL (87.28 and 86.29 mg, respectively) to a 100 mL volumetric flask and filling with deionized water to the mark. Further working tablet sample solutions in pH 6.0 PBS for each brand tablet were prepared from respective tablet stock solutions through serial dilution.

2.3.5.2. Human Blood Serum. 1.0 mL of serum from human blood serum collected from Tibebe Gion Referral Hospital at Bahir Dar City was transferred to a 25 mL conical flask, filled to the mark with pH 6.0 PBS, and stored in refrigeration for further analysis.

2.3.5.3. Human Urine. A human urine sample was obtained from a healthy volunteer in the laboratory and centrifuged at 4000 rpm for 10.0 min. 0.5 mL of the supernatant was transferred into a 25 mL flask and filled up to the mark with pH 6.0 PBS for further analysis.

3. RESULTS AND DISCUSSION

3.1. Synthesis of the CP_2RCoC Complex. *3.1.1. Synthesis Mechanism.* The CP_2RCoC complex was synthesized following a two-step (eqs 1 and 2) procedure using reso, $CoCl_2$, and phen as starting materials and using THF as the reaction medium (Scheme 1).

$$CoCl_2 + \text{resorcinol} \xrightarrow{\text{dry THF}} [CoRCl_2(THF)] \quad (1)$$

$$[CoRCl_2(THF)] + 2(\text{1,10-phenanthroline}) \rightarrow [CoP_2RCl]Cl + THF \quad (2)$$

The experimental results for the studied physicochemical properties of the synthesized two complexes are summarized in Table 1.

To prevent the kinetically beneficial competition of H_2O with reso, the synthetic method used anhydrous cobalt(II) chloride as a starting salt and dry THF as a reaction medium. The target complex, CP_2RCoC, showed different physical properties such as color, melting point, conductivity, and solubility from the intermediate complex, C_2RTCo, which has a nonelectrolytic behavior and a less polar character. These confirm the occurrence of the synthesis (Table 1). The intermediate complex was treated with phen, resulting in a complex of the composition CP_2RCoC, as determined by the Co content determination. The Co(II) and chloride content estimation experimental results of the synthesized complexes matched with the calculated value of the allocated structure for

https://doi.org/10.1021/acsomega.3c00170
ACS Omega 2023, 8, 15181−15192

Table 1. Summary of Studied Physicochemical Properties of C_2RTCo and CP_2RCoC

property	$[CoRCl_2(THF)]$	$[CoP_2RCl]Cl$
color	dark green	brick red
melting point (°C)	80	270
solubility	soluble in THF, DMF, acetone, methanol, ethanol, dichloromethane, water, acetonitrile, dimethylsulfoxide	soluble in water, methanol, ethanol, acetonitrile, dimethylsulfoxide
stability at room temperature	stable	stable
conductivity ($S\ cm^2\ mol^{-1}$)	0	153

the respective complex, C_2RTCo (Co: 37.53 (37.80), and Cl: 0 (0)); CP_2RCoC (Co: 19.33 (19.63), and Cl: 1.11 (1,18)).

3.1.2. Characterization of the Synthesized Complex. FT-IR and UV−vis spectroscopies were employed to characterize the synthesized complexes. In both approaches, changes like the appearance or disappearance of distinct peaks and peak intensity were considered as evidence for the synthesis of new complexes.

3.1.2.1. UV−Vis Spectroscopy. Figure SM1 depicts the electronic spectra of ligands, salt, and synthesized complexes in ethanol. The appreciable changes in the resonance bands following each reaction are a testimony to the occurrence of the intended reactions. One absorption band at 273 nm in the electronic spectra of reso has been ascribed to the $\pi \rightarrow \pi^*$ transition (Figure SM1B). This transition was observed to decrease in size in the spectrum of C_2RTCo, indicating that reso was coordinated with Co(II) (Figure S1C,D). The comparative decrease in the intensity of the characteristic absorption band of reso in C_2RTCo is attributed to the decrease in the mass proportion compared to its free form. The spectrum of phen shows two transition bands at 290 and 295 nm, which correspond to the $\pi \rightarrow \pi^*$ of C═C and −C═N, respectively (Figure SM1A). When it is coordinated to C_2RTCo, the band at 295 nm caused by −C═N's $\pi \rightarrow \pi^*$ disappears, showing that phen is coordinated through N of −C═N. Due to ligand-to-metal charge transfer (LMCT), the band at 226 nm in the spectra of CP_2RCoC (Figure S1E) is the blue-shifted appearance of the band at 240 nm in the spectrum of $CoCl_2$ (Figure S1C,E).

The band wavelength results from the UV−vis spectra and the proposed transition type for each band of the analyzed species are summarized in Table 2.

3.1.2.2. FT-IR Spectroscopy. The coordination of the ligands with the metal ion, which results in the hypothesized structure of the produced complexes, is strongly supported by the FT-IR spectra. Resorcinol was coordinated with Co(II) which is evident based on the υOH band's decrease in intensity relative to its C═C and the emergence of a new band at 540 cm^{-1} characteristic of υCo-O (Figure 1B,C). Since reso was coordinated by just one of its OH, the band resulting from υO-H is transformed into a broad one (Figure 1C). Furthermore, the broadening of the band in the range of 3400 to 3050 cm^{-1} is due to the presence of various vibrational frequencies of the two types of OH of reso as well as the υC-H (C−CH) of THF suggested the coordination of THF in addition to reso (Figure 1C). The bands at 1622 cm^{-1} (s) and 1588 cm^{-1} (s), characteristic for υC═C and υC═N in the free phen (Figure 1A) signaling at 1627 cm^{-1} (w) and 1589 cm^{-1} (w), respectively, in CP_2RCoC confirm the coordination of phen to the metal ion in C_2RTCo (Figure 1D). The presence of bands at 3370 and 1141 cm^{-1} due to υO−H and υC−O, respectively, indicates that reso remained in the complex after phen was coordinated (Table 3).

Table 2. UV−vis Spectral Data of the Salt, Ligands, and Synthesized Complexes and Proposed Transition Type

compound	λ_{max} (nm)	transition type
phen	290, 309, 323	$\pi \rightarrow \pi^*$(C═C), $\pi \rightarrow \pi^*$(C═N), n $\rightarrow \pi^*$(C═N)
reso	273	$\pi \rightarrow \pi^*$(C═C)
$CoCl_2$	240, 330	LMCT
	426	d−d($^4T_{1g} \rightarrow {}^4T_{2g}$)
C_2RTCo	273	$\pi \rightarrow \pi^*$ of C═C
CP_2RCoC	226	LMCT
	269	$\pi \rightarrow \pi^*$(C═C)
	290	n $\rightarrow \pi^*$(C═C) (phen)

3.2. Fabrication of Poly(CP_2RCoC)/GCE. During the attempt to deposit the poly(CP_2RCoC) film on the surface of the GCE potentiodynamically, the potential scan range and the number of scan cycles were the most important factors controlling the film thickness by inspecting the peak growth and optimization by investigation of the current response of the modified electrode toward the selected probe.

In this study, the current response of the modified electrode for CDL as a function of the number of scan cycles in the range of 10−25 was investigated (Figure S2). The oxidative peak current of CDL increased with the number of scan cycles, although with differing slopes (inset of Figure S2).

This experimental result is also supported by effective surface area enhancement and the electrocatalytic activity role of the optimum scan cycles (Figure S3). This enhanced electron transfer between the electrode and the analyte confirms the positive effects attained by poly(CP_2RCoC)/GCE with an increased peak current of the given probe. As a compromise between the current increment, analysis cost, R_{ct} value, and enhanced effective electrode surface area, 20 scan cycles were taken as the optimum number of polymerization cycles.

The potential scan window factors toward the deposition of the poly(CP_2RCoC) film on the surface of the GCE were also investigated. Figure S4 presents the response of poly-(CP_2RCoC)/GCE deposited in various potential windows for CDL. Hence, the optimized potential window for the cyclic voltammetric electropolymerization of the CP_2RCoC complex at the GCE was between −0.8 to +1.8 V. Similarly, the obtained result was further confirmed with electrical conductivity and effective surface area increments at the optimum potential window of −0.8 to +1.8 V relative to others (Figure S5).

Like the above parameters for the attempt of potentiodynamic deposition of the poly(CP_2RCoC) film on the surface of the GCE, the pH of the monomer solution affects the peak current of the analyte. Figure S6 presents the response of the poly(CP_2RCoC)/GCE for CDL prepared from 1.0 mM CP_2RCoC in PBS of various pHs (4.0, 7.0, and 10.0) all by scanning between −0.8 and +1.8 V. The poly(CP_2RCoC)/GCE fabricated from the monomer in pH 7.0 PBS showed the highest catalytic effect toward oxidation of CDL in terms of the current enhancement (inset of Figure S6).

https://doi.org/10.1021/acsomega.3c00170
ACS Omega 2023, 8, 15181−15192

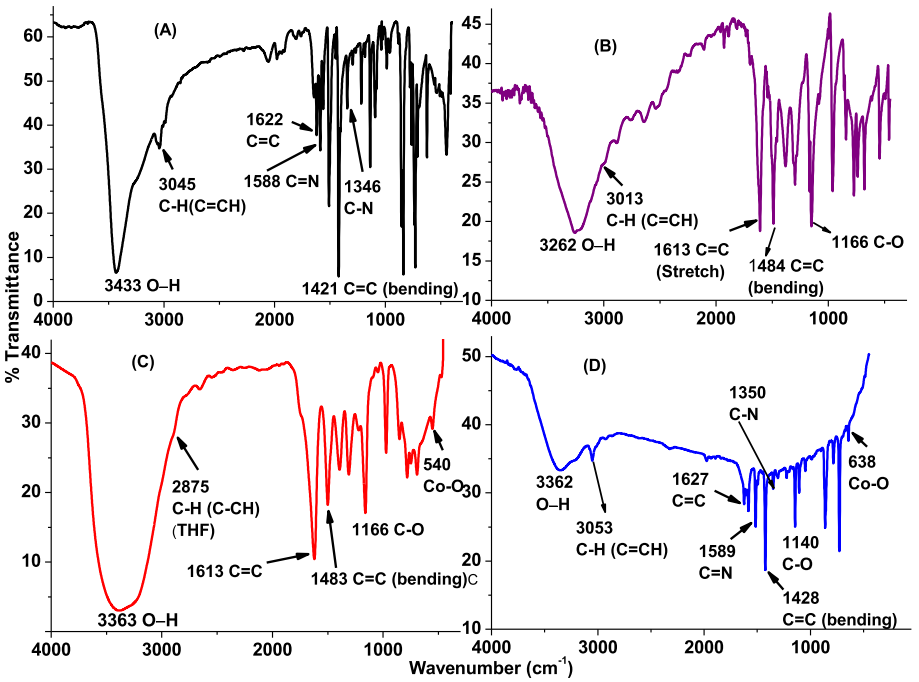

Figure 1. FT-IR spectra for (A) phen, (B) reso, (C) C_2RTCo, and (D) CP_2RCoC.

Table 3. Important Characteristic IR Bands of the Ligands and As-Synthesized Complexes and Proposed Vibrational Modes[a]

	absorption frequencies, cm^{-1}							
	νO–H (H_2O)	νC–H	νC=C	δC=C	νC=N	νC–N	δC–O	Co–O
phen	3433(s)	3045(w)	1622(m)	1421(s)	1588(s)	1346(s)		
reso	3262(s)	2885(w)	1613(s)				1166(s)	
C_2RTCo	3458–3195(b)	2875(w)	1613(s)	1483(s)		1389(m)	1152(m)	540(w)
CP_2RCoC	3362(s)	3053(w)	1627(m)	1428(s)	1589(m)	1350(w)	1140(m)	638(w)

[a] ν = stretching; δ = bending.

Therefore, poly(CP_2RCoC)/GCE synthesized from CP_2RCoC in pH 7.0 PBS scanned between −0.8 and +1.8 V for 20 cycles (Figure 2) was selected for determination of CDL in tablet, human blood serum, and urine samples.

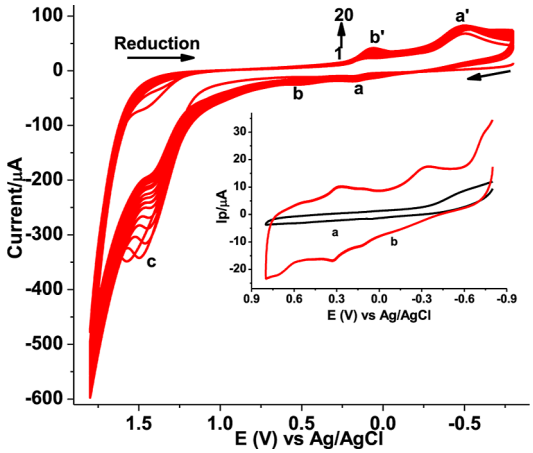

Figure 2. Repetitive cyclic voltammograms of the GCE in pH 7.0 PBS containing 1.0 mM CP_2RCoC scanned between −0.8 and +1.8 V at a scan rate of 100 mV s^{-1} for 20 cycles. Inset: Cyclic voltammograms of stabilized (a) bare GCE and (b) poly(CP_2RCoC)/GCE in 0.5 M H_2SO_4 between −0.8 and +0.8 V.

Increasing the peak current of the anodic peak (*a*, *b*, and *c*) centered at about +181, +508, and +1480 mV, respectively, and cathodic peak (*a'* and *b'*) −504 and +63 mV, respectively, with increasing scan cycles confirmed redox polymer film deposition at the electrode surface. In contrast to the cyclic voltammogram of the bare GCE in 0.5 M H_2SO_4 containing no analyte (curve *a* of inset) which showed only a broad reductive peak above −600 mV ascribed to molecular oxygen reduction, the appearance of multiple oxidative and reductive peaks on the cyclic voltammogram of the poly(CP_2RCoC)/GCE (curve *b* of inset) in the same further confirmed the electroactivity of the polymer film deposited on the electrode surface.

The anodic peaks (*a* and *b*) observed at +181 and +508 mV are believed to be characteristics of the polymer film deposited, which may be through radical cation-induced polymerization due to electron delocalization within the phen and reso ring,[13,18] and that at +1480 mV was assigned to the oxidation of Co(0) to Co(II), while the reductive peaks centered at about −504 and +63 mV were observed due to the reduction process from Co(II) to Co(I) and Co(I) to Co(0), respectively.[18,27] However, the authors still are not able to propose the exact mechanism of the electropolymerization of the mixed ligand-based Co(II) complexes in this study.

3.3. Electrochemical Characterization of the Modified Electrode. *3.3.1. Cyclic Voltammetric Characterization.* CV was used to follow the synthesis of a new material based on the features of the resulting voltammograms for both CDL and

https://doi.org/10.1021/acsomega.3c00170
ACS Omega 2023, 8, 15181−15192

$Fe(CN)_6^{3-/4-}$. Figure S7 presents the repetitive cyclic voltammograms of the GCE in a solution of (A) Co(II) salt, (B) phen, (C) reso, (D) C_2RTCo, and (E) CP_2RCoC. The voltammograms of each electropolymerization of the GCE showed distinct oxidative and reductive peaks with observed potential shifts to the other, confirming the conversion of salt and the ligands to the complex.

Figure 3 shows the CV response of $Fe(CN)_6^{3-/4-}$ at various forms of the GCE. In contrast to the bare GCE (a) and

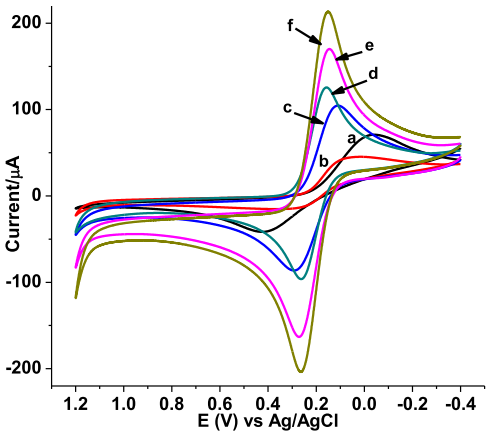

Figure 3. Cyclic voltammograms of (a) GCE, (b) poly(phen)/GCE, (c) poly(reso)/GCE, (d) electrodeposited (Co(0))/GCE, (e) poly(C_2RTCo)/GCE, and (f) poly(CP_2RCoC)/GCE in pH 7.0 PBS containing 10.0 mM $(Fe(CN)_6)^{3-/4-}$ and 0.1 M KCl at a scan rate of 100 mV s^{-1}.

poly(phen)/GCE (b), other modified GCEs showed pairs of peaks with comparably reduce peak−peak potential separation and improved current intensity.

In general, the peak−peak separation of the electrodes for the probe was in the order bare GCE (ΔE 415) > poly(phen)/GCE (ΔE 225) > poly(reso)/GCE (ΔE 170) > poly(C_2RTCo)/GCE (ΔE 109) > poly(Co(II))/GCE (ΔE 98) > poly(CP_2RCoC)/GCE (ΔE 92 mV) the current response was poly(CP_2RCoC)/GCE > poly(C_2RTCo)/GCE > poly(Co(0))/GCE > poly(reso)/GCE > bare GCE > poly(phen)/GCE. Meanwhile, the peak−peak separation is mainly associated with the conductivity of the surface material; the peak current intensity could be ascribed to the resulting effective surface area of the electrode. Hence, the least current response observed at the poly(phen)/GCE might be due to possible electrostatic repulsion between the negatively charged poly(phen)/GCE (pKa = 4.86) and $(Fe(CN)6)^{3-/4-}$.[17]

The active surface areas of the working electrodes were estimated using the slope value of the plot of I_{pa} versus $\nu^{1/2}$ for $(Fe(CN)_6)^{3-/4-}$, based on the Randles−Sevcik equation (eq 3).[28]

$$I_{pa} = 2.69 \times 10^5 n^{3/2} A D^{1/2} \nu^{1/2} C_o \quad (3)$$

where I_{pa}—the anodic peak current, n—number of electron transfer, A—active surface area of the electrode, D—diffusion coefficient, C_o—bulk concentration of $Fe(CN)_6^{3-/4-}$, and ν—scan rate.

The calculated effective surface areas of the studied electrodes are presented in Table 4. Thus, the enhanced current of the poly(CP_2RCoC)/GCE for the probe in Figure S8 might be ascribed to its much improved effective surface

Table 4. Summary of Calculated Effective Surface Area of the Studied Electrodes

electrode	slope of $(\nu)^{1/2}$ *vs* I_{pa}	electrode surface area/cm^2
GCE (A)	4.0	0.054
poly(phen)/GCE (B)	2.1	0.028
poly(reso)/GCE (C)	8.1	0.109
poly(Co(II))/GCE (D)	10.6	0.143
poly(C_2RTCo)/GCE (E)	15.5	0.209
poly(CP_2RCoC)/GCE (F)	20.4	0.275

area, which is nearly 5 times larger than that of the unmodified GCE.

3.3.2. Electrochemical Impedance Spectroscopic Characterization. EIS was used to verify the electrode modification and the interfacial properties of both the GCE and poly(CP_2RCoC)/GCE. The Nyquist plots (Figure 4) for all the

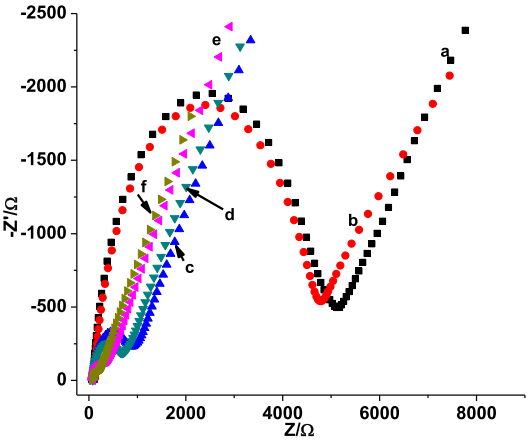

Figure 4. Nyquist plot of (a) bare GCE, (b) poly(phen)/GCE, (c) poly(reso)/GCE, (d) electrodeposited Co(0)/GCE, (e) poly(C_2RTCo)/GCE, and (f) poly(CP_2RCoC)/GCE in pH 7.0 PBS containing 10.0 mM $[Fe(CN)_6]^{3-/4-}$ and 0.1 M KCl in the frequency range: 0.01−100,000 Hz, amplitude: 0.01 V, and potential: 0.23 V.

electrodes exhibited a semicircle with varying diameter at the high-frequency region [represents the charge transfer resistance (R_{ct}) of the electrode] and low-frequency region representing the diffusion of the electroactive species from the bulk to the solution−electrode interface.[13]

Table S1 presents the summary of circuit elements including solution resistance (R_s), R_{ct}, and double-layer capacitance (C_{dl}) for each studied electrode as calculated from the respective Nyquist plot using eq 4.

$$C_{dI} = \frac{1}{2\pi R_{ct} f} \quad (4)$$

where C_{dI}—double-layer capacitance, f—frequency corresponding to the imaginary resistance at its highest value, and R_{ct}—charge transfer resistance.

The R_{ct} value of the unmodified GCE is the highest (5427 Ω, curve *a*) followed by the value for the poly(phen)/GCE (4950 Ω, curve *b*) which could be attributed to the Coulombic force of repulsion between the negatively charged $[Fe(CN)_6]^{3-}$ and poly(phen) film. Among the studied electrodes, the R_{ct} value for the poly(CP_2RCoC)/GCE was the least significantly decreased, which was (186.9 Ω, curve *f*), demonstrating that the CP_2RCoC film on the GCE surface

https://doi.org/10.1021/acsomega.3c00170
ACS Omega 2023, 8, 15181−15192

greatly enhanced the conductivity and hence the electron transfer rate between the substrate and the analyte. The observed significantly reduced R_{ct} value added with the enhanced peak current response for $Fe(CN)_6^{3-/4-}$ and significantly increased effective surface area confirmed the successful modification of the GCE by the poly(CP_2RCoC) film.

The surface roughness (R_F) of poly(CP_2RCoC)/GCE and the apparent heterogeneous electron transfer rate constant (k^0) value were estimated by using eqs 5 and 6, respectively.[22,28]

$$R_F = \frac{C_{dI}}{C_S} \tag{5}$$

$$k^0 = \frac{RT}{F^2ACR_{ct}} \tag{6}$$

where R—molar gas constant (8.314 J mol^{-1} K^{-1}), T—temperature (298 K), F—Faraday constant (96,485 C mol^{-1}), A—surface area of the electrode, C—concentration of $[Fe(CN)_6]^{3-/4-}$, and C_{dI} and C_S—electrochemical double-layer capacitance of a planar and smooth electrode surface of the same material measured under the same conditions, respectively.

The slopes of bare and poly(CP_2RCoC)-modified GCE surfaces are given (Figure S8A,F, respectively); a roughness factor of 5.1 of the poly(CP_2RCoC)/GCE is obtained. Similarly, the k^0 values obtained for the poly(CP_2RCoC)/GCE are 5.7 times higher than those for the unmodified GCE, clearly indicating that the electrochemical activity for the redox probe is enhanced on the CP_2RCoC-modified electrode surface.

3.4. Cyclic Voltammetric Investigation of CDL.

3.4.1. Electrochemical Behavior of CDL at Poly(CP_2RCoC)/GCE. The obtained characterization results are the most important indicators for the surface of the poly(CP_2RCoC)/GCE to exhibit a catalytic role. The electrochemical behavior of CDL at the unmodified GCE and five modified GCEs was studied using CV (Figure 5).

However, CDL shows a single irreversible oxidation peak at all the studied electrodes irrespective of the type of electrode.

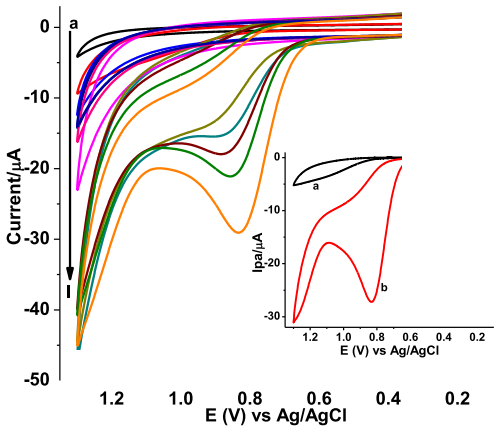

Figure 5. Cyclic voltammograms of bare GCE (a,g), poly(phen)/GCE (b,h), electrodeposited (Co(0))/GCE (c,i), poly(reso)/GCE (d,j), poly(C_2RTCo)/GCE (e,k), and poly(CP_2RCoC)/GCE (f,l) in pH 7.0 PBS containing 1.0 mM CDL at a scan rate of 100 mV s^{-1}. Inset: blank corrected cyclic voltammograms of (a) unmodified GCE and (b) poly(CP_2RCoC)/GCE.

Much reduced potential with a 7-fold current enhancement at the poly(CP_2RCoC)/GCE (curve *b* of inset) confirmed the catalytic effect of the poly(CP_2RCoC)/GCE film toward oxidation of CDL. The absence of any reduction peak on the reverse scan indicated that the oxidation of CDL is irreversible at both the unmodified and modified GCE.

Moreover, the observed current and potential advantages for CDL at poly(CP_2RCoC)/GCE compared to the response at poly(phen)/GCE, Co(0)/GCE, poly(reso)/GCE, and poly(C_2RTCo)/GCE verified the suitability of poly(CP_2RCoC)/GCE for determination of CDL.

3.4.2. Effect of Scan Rate on the I_{pa} and E_{pa} of CDL. The influence of the scan rate on the peak potential and peak current was studied to check the irreversibility of the oxidation reaction and investigate the rate-determining step during the reaction of CDL at poly(CP_2RCoC)/GCE. Figure 6 presents voltammograms of 1.0 mM CDL in pH 7.0 PBS at poly(CP_2RCoC)/GCE in the scan rate range of 20−300 mV s^{-1}.

The lower correlation coefficient of the plot of oxidative peak current versus the scan rate (R^2 = 0.96934) (Figure 6B) than with the square root of scan rate (R^2 = 0.99685) (Figure 6C) indicated that the oxidation of CDL at the poly(CP_2RCoC)/GCE was predominantly diffusion-controlled.[7,13,25] This was also confirmed by the slope of 0.61 for the plot of log (peak current) versus log (scan rate) (Figure 6D), which is exactly in agreement with the ideal value.[7] However, the observed peak potential shift of CDL with increasing scan rate (Figure 6A) suggests the irreversibility of the oxidation of CDL.[7,18]

The number of electrons transferred during the oxidation of CDL at the poly(CP_2RCoC)/GCE was determined from CV data. For an irreversible process, the value of αn was determined from the difference between the peak potential (E_p) and the half-wave potential ($E_{p1/2}$) by employing eq 7.[28]

$$E_p - E_{p1/2} = \frac{48}{\alpha n} \tag{7}$$

where α is the charge transfer coefficient and n is the number of electrons transferred.

Taking E_p and $E_{p1/2}$ from the CV data at a scan rate of 100 mV s^{-1} to be 907 and 824 mV, respectively, the value of αn was calculated as 0.58. Considering α for the totally irreversible electrode process to be 0.50,[30] the number of electrons (n) transferred in the oxidation of CDL at the surface of poly(CP_2RCoC)/GCE was estimated to be 1.16 (~1.0), which agreed with that in refs7 and 23.

The relationship between E_p and ln ν for an irreversible process obeys eq 8.[28]

$$E_p = E^O + \frac{RT}{(1-\alpha)nF}\left\{0.780 + \ln\left(\frac{D_R^{1/2}}{k^0}\right) + \ln\left[\frac{(1-\alpha)nF\nu}{RT}\right]^{1/2}\right\} \tag{8}$$

where E_P is the peak potential, E^o is the formal potential, α is the electron transfer coefficient, k^0 (s^{-1}) is the electrochemical rate constant, and the other parameters have their usual meanings.

From the slope value of 0.021 for the fitted line (E_{pa} (V) = 0.81 + 0.021 ln ν) of the curve of the plot of E_p versus ln (scan

https://doi.org/10.1021/acsomega.3c00170
ACS Omega 2023, 8, 15181−15192

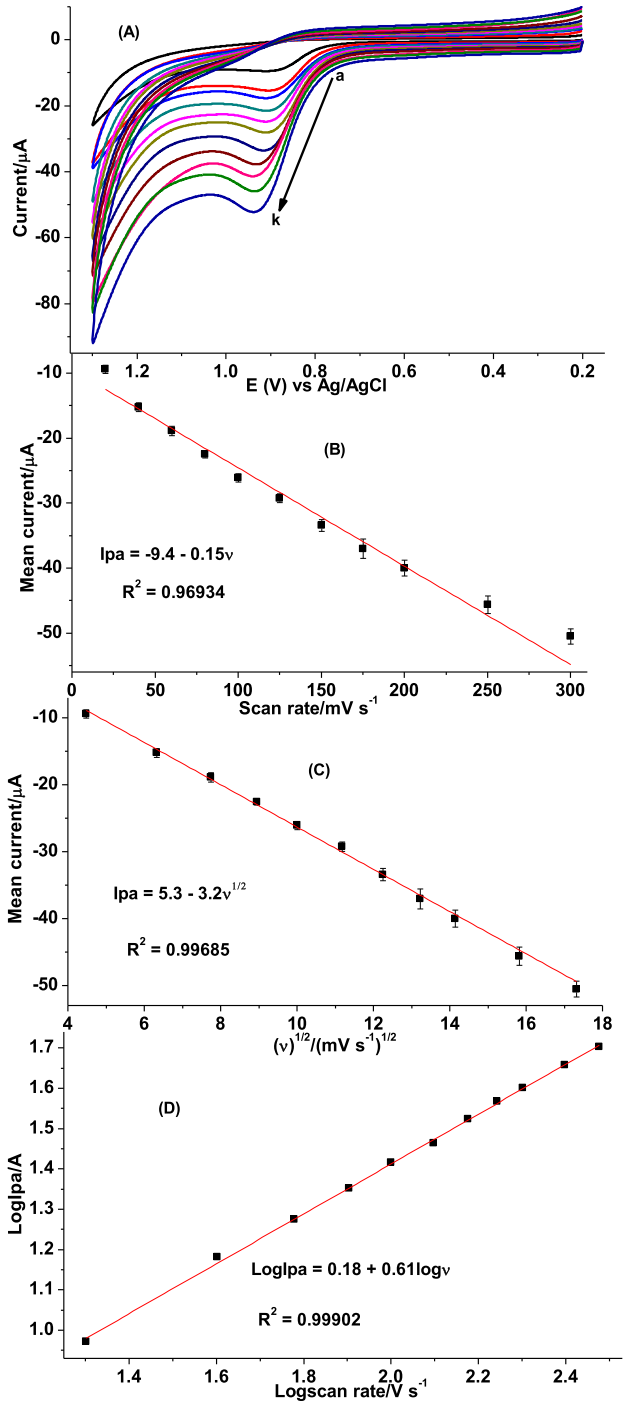

Figure 6. (A) Cyclic voltammograms of poly(CP_2RCoC)/GCE in pH 7.0 PBS containing 1.0 mM CDL at various scan rates (a–k: 20, 40, 60, 80, 100, 125, 150, 175, 200, 250, and 300 mV s^{-1}, respectively), (B) plot of I_{pa} *vs* ν, (C) plot of I_{pa} *vs* $\nu^{1/2}$, and (D) plot of log I_{pa} *vs* log ν.

rate) (Figure S9), the value of $n(1-\alpha)$ at the experimental temperature of 25 °C calculated using eq 8 was 0.64. Taking the one electron for oxidation of CDL calculated using eq 7, the electron transfer coefficient (α) was estimated to be 0.36, confirming the irreversibility of the oxidation of CDL.[7,28]

3.4.3. Effect of pH on I_{pa} and E_{pa} of CDL. The effect of pH on the peak current and peak potential of electroactive species at an electrode is used to evaluate the participation of proton in the reaction, proton/electron ratio, and rationalize the type of interaction between the analyte and surface of the electrode.[29]

The observed oxidation peak current of CDL at poly-(CP_2RCoC)/GCE increased with the pH value from 4.0 to 6.0 and then decreased beyond the pH value of 6.0 (curve *a* of Figure 7B), making pH 6.0 the optimum pH for further

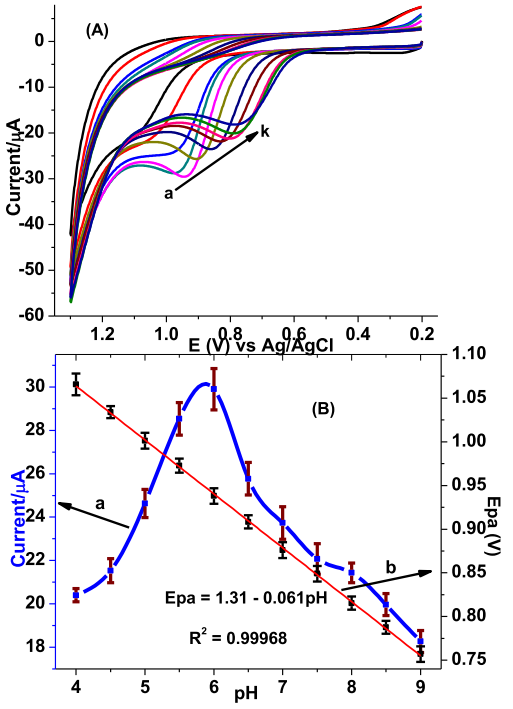

Figure 7. (A) Cyclic voltammograms of poly(CP_2RCoC)/GCE in PBS of various pHs (a–i: 4.0, 4.5, 5.0, 5.5, 6.0, 6.5, 7.0, 7.5, 8.0, 8.5, and 9.0, respectively) containing 1.0 mM CDL; (B) plot of (a) peak current and (b) peak potential *vs* pHs in the entire pH range.

voltammetric investigations of CDL. The increasing current trend could partly be attributed to the Coulombic forces of interaction exhibited between the electrode modifier (poly-(CP_2RCoC)) film (pka = 4.86 and 9.15, phen and reso, respectively),[13,18,23] and CDL (pka = 2.48, 7.37, and 9.64).[7,31] Hence the observed increase of current with pH from 4.0 to 6.0 may be accounted for the possible attraction between the cationic carboxylic acid (pka 2.48) for CDL and the negatively charged modifier film.

The peak potential shift in the negative direction with pH values varies from 4.0 to 9.0, indicating proton participation in the oxidation process (Figure 7A),[13,23] the slope of 0.061 V in the plot of peak potential versus pH of the PBS (curve *b* of Figure 7B), which is very close to the ideal Nernst value (0.059 V/pH), showed involvement of protons and electrons in a 1:1 ratio during the reaction process.[7,13,25]

Based on the calculated kinetic parameters using eqs 7 and 8 and the slope of I_{pa} versus pH, a reaction mechanism for the oxidation of CDL at poly(CP_2RCoC)/GCE was proposed (Scheme S2) which is in agreement with the mechanism in previously reported works.[7,25]

3.5. SWV Investigation of CDL at Poly(CP_2RCoC)/GCE.

Due to higher sensitivity, lower LoD, and better resolution of SWV, it is more powerful in discriminating Faradaic current from the non-Faradaic current than CV,[18,23] and it was used for quantification of CDL in various real samples.

https://doi.org/10.1021/acsomega.3c00170
ACS Omega 2023, 8, 15181−15192

Figure 8 shows SWVs of 1.0 mM CDL in pH 6.0 PBS at poly(CP_2RCoC)/GCE and unmodified GCE. The oxidative

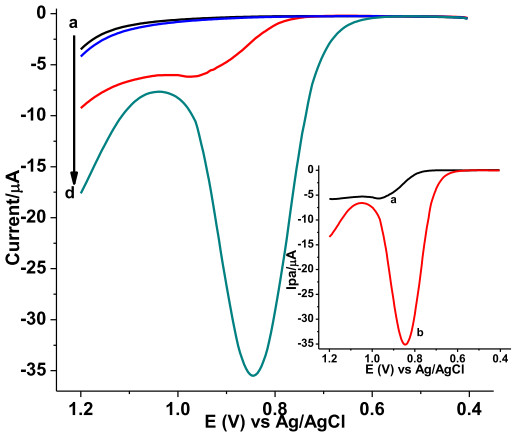

Figure 8. SWVs of unmodified GCE (a,b) and poly(CP_2RCoC)/GCE (c,d) in pH 6.0 PBS in the absence (a,c) and presence (b,d) of 1.0 mM CDL at step potential: 4 mV, amplitude: 25 mV, and frequency: 15 Hz. Inset: blank subtracted SWVs of (a) bare GCE and (b) poly(CP_2RCoC)/GCE.

peak at the poly(CP_2RCoC)/GCE with a much reduced potential and a 7-fold current enhancement (curve *b* of inset) (35.4 μA and 844 mV) than that at the unmodified GCE (5.61 μA and 971 mV) (curve *a* of inset) signified the catalytic role of the modifier toward the oxidation of CDL.

Selected SWV parameters (step potential, square-wave amplitude, and frequency) were optimized for further analysis. Figure SM10 presents the SWVs at different step potentials (A), amplitudes (B), and square-wave frequencies. The parameters were optimized by making a compromise between the peak current increment and the accompanied peak broadening. Hence, 6 mV, 35 mV, and 20 Hz were taken as the optimum step potential, amplitude, and frequency, respectively.

3.6. Calibration Curve and Method Detection Limit. Under the optimal solution and parameters, the calibration curve of CDL was constructed in the concentration range of 1.0×10^{-7}–3.0×10^{-4} M (inset of Figure 9), with an LoD (S/N = 3, for n = 7) and LoQ of 4.3×10^{-9} M and 1.4×10^{-8} M, respectively. The low associated % RSD values below 3.75% for triplicate measurement showed precision and accuracy and hence validated the applicability of the proposed method based on the mixed-ligand Co(II) complex as an electrode modifier for determination of CDL in tablet formulations, human blood serum, and urine samples.

3.7. SWV Determination of CDL in Real Samples Using Poly(CP_2RCoC)/GCE. *3.7.1. Tablet Sample.* The applicability of the developed method for the determination of the two tablet brands (Drox and Cefacef) for determination of their CDL content and comparing the detected levels with the company's label prepared following the procedure under Section 2.3.5.1 was investigated.

The SWVs for 20.0 and 40.0 μM of CDL for each tablet brand are presented in Figure S11, and the detected amount of CDL in each sample is summarized in Table 5.

As can be seen from the table, the detected content of CDL in the range of 97.25–100.00% of what was expected with a % RSD value below 2.5% showed the accuracy of the developed method and hence validated the applicability of the method for

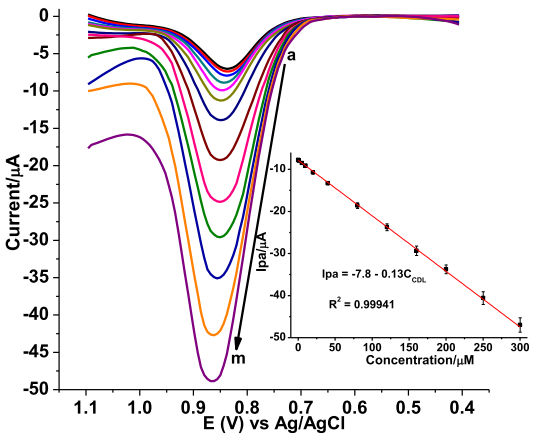

Figure 9. Blank corrected SWVs of poly(CP_2RCoC)/GCE in pH 6.0 PBS for various concentrations of CDL (a–m: 0.1, 0.5, 1.0, 5.0, 10.0, 20.0, 40.0, 80.0, 120.0, 160.0, 200.0, 250.0, and 300.0 μM, respectively) at step potential: 6 mV, amplitude: 35 mV, and frequency: 20 Hz. Inset: plot of I_{pa} (mean ± % RSD as error bar) *vs* concentration of CDL.

determination of CDL in a tablet sample with the complex matrix.

3.7.2. Human Blood Serum Sample. In the analyzed human serum sample, the absence of a peak at the characteristic potential of CDL (Figure 10a) indicates the absence of CDL, but the appearance of a peak at a potential away from the characteristic potential for CDL indicates the presence of a creatinine electroactive substance in the serum sample (Figure 10a) similar to the reported literature.[23]

3.7.3. Human Urine Sample. Figure SM12 presents blank corrected SWVs for human urine prepared following the procedure described under Materials and Methods. While the absence of a peak at the characteristic potential of CDL indicates the absence of CDL in the analyzed urine sample, the appearance of a peak at a potential away from the characteristic potential for CDL indicates the presence of creatinine in the analyzed urine sample (Figure S12b) similar to the previous work.[23]

3.8. Validation of the Developed Method. *3.8.1. Recovery Study. 3.8.1.1. Human Blood Serum Sample.* Spiking of a sample of blood serum was carried out by spiking the serum sample analyzed under 3.7.2 with 20.0, 40.0, 80.0, and 120.0 μM CDL standard solutions (Figure 10). The serum sample revealed a peak centered at about 647 mV (peak a) with the same current intensity without the level of spiked CDL, indicating that the peak is not for CDL. On the other hand, the appearance of a new peak at the characteristic potential of CDL (≈880 mV) whose current intensity increased with the amount of CDL spiked in the serum samples (curves *b*–*e*) confirmed that the peak in the unspiked serum is not CDL. The spike recovery percent of CDL in human blood serum samples in the range of 99.20–100.39% (Table S2) with a % RSD value below 3.7% showed selectivity and accuracy of the method for determination of CDL in the blood serum sample.

3.8.1.2. Human Urine Sample. To check the applicability of the developed SWV method based on poly(CP_2RCoC)/GCE for CDL determine in urine samples, recovery studies by spiking CDL in analyzed urine sample solutions were conducted (Figure S12). Peak (*A*) of the urine sample with exactly constant current intensity regardless of the level of

https://doi.org/10.1021/acsomega.3c00170
ACS Omega 2023, 8, 15181–15192

Table 5. Summary of Detected CDL Content and Percent Detected as Compared to the Nominal Value for Each Analyzed Tablet Brand

			detected CDL in		
tablet brand	labeled CDL (mg/tablet)	nominal CDL in the sample (μM)	sample (μM)[a]	tablet (mg/tablet)	detected CDL (%)[b]
drox	500	20.0	19.92 ± 0.025	498.0	99.6 ± 2.5
		40.0	40.00 ± 0.024	500.0	100.0 ± 2.4
cefacef	500	20.0	19.61 ± 0.025	490.25	98.05 ± 2.5
		40.0	38.90 ± 0.023	486.25	97.25 ± 2.3

[a]Detected mean CDL ± RSD. [b]Detected mean % CDL ± % RSD.

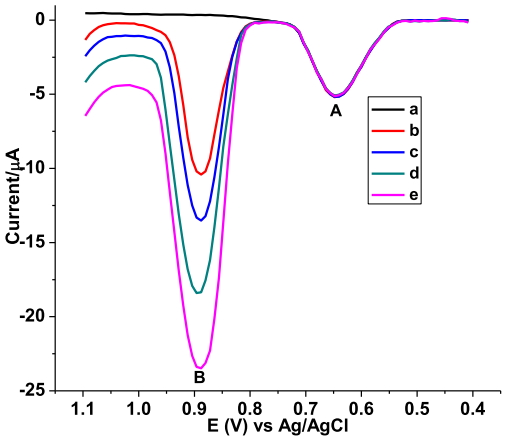

Figure 10. Blank-subtracted SWV of poly(CP_2RCoC)/GCE in pH 6.0 PBS containing the (a) unspiked serum sample, (b) a + 20.0 μM, (c) a + 40.0 μM, (d) a + 80.0 μM, and (e) a + 120.0 μM standard CDL solutions.

spiked CDL indicated that the peak was not for CDL. On the other hand, the appearance of a new peak (peak *B*) at the characteristic potential of CDL whose current intensity increased with the amount of CDL spiked in the urine samples (curves *b*–*d*) confirmed that the peak in the unspiked urine was not for CDL. The percent spike recovery of CDL in human urine of 98.10–99.99% (Table S3) with a % RSD value below 3.2% confirmed the applicability of the method for the determination of CDL in the urine sample.

3.8.1.3. Tablet Samples. The spiking recovery test of the tablet sample was conducted by spiking Drox brand tablet samples with different concentrations of standard CDL (0.0, 20.0. 40.0, 80.0, and 120.0) (Figure S13). As shown in Table S4, recovery results in the range 98.85–101.3% with a % RSD value below 3.1% confirmed the precision of the method for the determination of CDL in tablet formulations.

3.8.2. Interference Study. To evaluate the commercial importance of the developed sensor, investigating the selectivity of the developed sensor toward possible interfering substances for the determination of CDL in real samples like pharmaceutical formulations, human blood serum, and urine samples is important. For the interference studies, drugs which could be present in the CDL tablet or having structural similarities with CDL, commonly administrated together with CDL and expected to be found in real samples, were selected.

The effect of the selected potential interferent in the tablet sample was investigated at its various concentrations of ascorbic acid, ampicillin (AMP), cephalexin (CLN), and cloxacillin (CLOX) (Figure S14A–D). The claimed CDL level in the tablet sample was detected with an associated error under 4.74% (Table S5) in the presence of interfering molecules, suggesting that the detection of CDL in the tablet sample at poly(CP_2RCoC)/GCE is not disturbed by the existence of interfering substances, which is important for the commercial viability of a developed sensor.

3.8.3. Reproducibility and Stability Studies. For the quality of any sensor, reproducibility and stability evaluation are very important. In this regard, we have tested our developed sensor (poly(CP_2RCoC)/GCE) for reproducibility by checking the current responses at five separate electrodes prepared using a similar fabrication process, which showed the % RSD < 2.82% (n = 5) (Figure S15A). The long-term stability of the developed sensor for five successive SWV measurements recorded at an interval of 1 week for 6 weeks with an error of only 3.16% (% RSD) (Figure S15B) suggested the reproducibility and stability of the developed sensor.

3.9. Comparison of the Present Method with Previously Reported Methods. The performance of the developed method in this study was compared with previously reported work in terms of the nature of the substrate used for modification, linear dynamic range, and LoD.

The present method based on a synthesized novel mixed-ligand complex-modified electrode (poly(CP_2RCoC)/GCE) provides the least LoD with a wider linear dynamic range than the other reported methods (Table 6). Therefore, the present method using the novel modifier can be an excellent candidate for the determination of CDL in various real samples.

4. CONCLUSIONS

A chemical sensor for the detection of CDL in pharmaceutical tablet formulations, human blood serum, and urine samples was developed using a cheap and nontoxic GCE modifier ([CoP_2RCl]Cl) prepared by a simple method. This technique employs aqueous solvents, inexpensive instrumentation, and short analysis time and is eco-friendly. The cyclic voltammetric and electrochemical impedance spectroscopic investigation

Table 6. Performance of the Developed Method in Contrast to Selected Reported Works

substrate	modifier	method	dynamic range (μM)	LoD (μM)	ref
GCE	poly(Alz)	DPV	0.1–100	0.0081	2
GCE	AuNP/MWCNT	amperometry	2.0–10.0	0.22	25
GCE	nano-Ag-APME	AdSWV	0.033–0.304 & 10–70	0.01 & 0.03	26
GCE	poly(CP_2RCoC)	SWV	0.1–300.0	0.0043	this work

https://doi.org/10.1021/acsomega.3c00170
ACS Omega 2023, 8, 15181–15192

results confirmed the deposition of an electroactive poly-(CP_2RCoC) film on the surface of GCE that increased the surface area and conductivity of the electrode surface. The poly(CP_2RCoC)/GCE possessed excellent electrocatalytic activity toward the oxidation of CDL. The square-wave voltammetric method based on poly(CP_2RCoC)/GCE was used for the determination of CDL in two brands of tablet formulations, human blood serum, and urine samples with a complex matrix. A wide linear dynamic range, reasonably low detection limit, excellent spike and interference recovery results, and excellent reproducibility and stability validated the applicability of the developed method for the determination of CDL in various real samples. The CDL content of the studied tablet samples ranged between 97.25 and 100.00% of their nominal labels, confirming the efficiency of the developed sensor. In contrast to the previously reported sensors, our developed method showed excellent performance for the determination of CDL in samples with complex matrixes including pharmaceutical, urine, and serum samples.

■ ASSOCIATED CONTENT

Supporting Information

The Supporting Information is available free of charge at https://pubs.acs.org/doi/10.1021/acsomega.3c00170.

Chemical structures; UV−vis spectra, cyclic voltammograms; square-wave voltammograms; Nyquist plot of different number of polymerization scan cycles; Nyquist plot of different potential scan windows; tables of calculated circuit elements for the studied electrodes; plot of mean oxidative potential *vs* ln (scan rate); proposed oxidative reaction mechanism for CDL; spike recovery results of CDL in human blood serum and urine samples; and percent interference recovery results of CDL in tablet samples (PDF)

■ AUTHOR INFORMATION

Corresponding Author

Atakilt Abebe − *Department of Chemistry, College of Science, Bahir Dar University, Bahir Dar H9FX+Q62, Ethiopia;* orcid.org/0000-0002-5496-664X; Email: atakiltabebe1@gmail.com

Authors

Adane Kassa − *Department of Chemistry, College of Natural and Computational Sciences, Debre Markos University, Debre Markos 269, Ethiopia; Department of Chemistry, College of Science, Bahir Dar University, Bahir Dar H9FX+Q62, Ethiopia*

Amare Benor − *Department of Physics, College of Science, Bahir Dar University, Bahir Dar H9FX+Q62, Ethiopia*

Getinet Tamiru Tigineh − *Department of Chemistry, College of Science, Bahir Dar University, Bahir Dar H9FX+Q62, Ethiopia*

Complete contact information is available at: https://pubs.acs.org/10.1021/acsomega.3c00170

Author Contributions

Data curation: A.K. and A.A. Data analysis: A.K., A.A., G.T., and A.B. Methodology: A.K. and A.A. Supervision: A.A. Original draft writing: A.K. and A.A. Writing−review and editing: A.K., A.A., G.T., and A.B.

Funding

This research did not receive any specific grant from funding agencies in the public, commercial, or not-for-profit sectors.

Notes

The authors declare no competing financial interest.

■ ACKNOWLEDGMENTS

The Ethiopian Food and Drug Administration Authority (EFDA), Addis Pharmaceutical Factory (APF), and Bahir Dar University's College of Science are acknowledged by the authors for providing standards and access to laboratory resources, respectively. SIDA (the Swedish International Development Cooperation Agency) through the ISP (International Science Programme, Uppsala University) is acknowledged for financial support.

■ REFERENCES

(1) Kirankumar, S. V.; Jose Gnana Babu, C.; Sowmya, H. G. Validated AUC method for the spectrophotometric estimation of cefadroxil in bulk and tablet dosage form. *Int. J. Chem. Pharm. Anal.* **2020**, *7*, 226−230.

(2) Arias, C. A.; Murray, B. E. Antibiotic-resistant bugs in the 21st century—a clinical super-challenge. *N. Engl. J. Med.* **2009**, *360*, 439−443.

(3) Lofrano, G.; Libralato, G.; Adinolfi, R.; Siciliano, A.; Iannece, P.; Guida, M.; Giugni, M.; Volpi Ghirardini, A.; Carotenuto, M. Photocatalytic degradation of the antibiotic chloramphenicol and effluent toxicity effects. *Ecotoxicol. Env. Saf.* **2016**, *123*, 65−71.

(4) Carlet, J.; Pulcini, C.; Piddock, L. J. Antibiotic resistance: a geopolitical issue. *Clin. Microbiol. Infect.* **2014**, *20*, 949−953.

(5) Wang, Q.; Wang, D.; Wang, J.; Cui, Y.; Xu, H. Recent progress and novel perspectives of electrochemical sensor for cephalosporins detection. *Int. J. Electrochem. Sci.* **2019**, *14*, 8639−8649.

(6) *Wilson and Gisvold's Textbook of Organic Medicinal and Pharmaceutical Chemistry*, 12th ed.; Beale, J. M., Block, J., Eds.; R. Hill, 2011.

(7) Kassa, A.; Amare, M. Highly selective and sensitive differential pulse voltammetric method based on poly (Alizarin)/GCE for determination of cefadroxil in tablet and human urine samples. *Arab. J. Chem.* **2021**, *14*, 103296−103312.

(8) Marco, B.; Kogawa, A.; Salgado, H. New, green and miniaturized analytical method for determination of cefadroxil monohydrate in capsules. *Drug Anal. Res.* **2019**, *3*, 23−28.

(9) Rahim, N.; Naqvi, S. B.; Shakeel, S.; Iffat, W.; Muhammad, I. N. Determination of cefadroxil in tablet/capsule formulations by a validated reverse phase high performance liquid chromatographic method. *Pak. J. Pharm. Sci.* **2015**, *28*, 1345−1349.

(10) Rao, K. G.; Uma, B.; Shankar, B.; Naik, B. M. Development and validation of RP-HPLC method for the estimation of cefadroxil monohydrate in bulk and its tablet dosage form. *J. Adv. Pharm. Edu. Res.* **2014**, *4*, 71−74.

(11) Nagarajan, J. S. K.; Vimal, C. S.; George, R.; Dubala, A. Simultaneous pharmacokinetic assessment of cefadroxil and clavulanic acid in human plasma by LC−MS and its application to bioequivalence studies. *J. Pharm. Anal.* **2013**, *3*, 285−291.

(12) Sanz, C. G.; Serrano, S. H.; Brett, C. M. Electrochemical characterization of cefadroxil β-lactam antibiotic and Cu (II) complex formation. *J. Electroanal. Chem.* **2019**, *844*, 124−131.

(13) Kassa, A.; Abebe, A.; Amare, M. Synthesis, characterization, and electropolymerization of a novel Cu (II) complex based on 1, 10-phenanthroline for electrochemical determination of amoxicillin in pharmaceutical tablet formulations. *Electrochim. Acta* **2021**, *384*, 138402−138415.

(14) Kassa, A.; Amare, M. Poly (4-amino-3-hydroxynaphthalene-1-sulfonic acid) modified glassy carbon electrode for square wave voltammetric determination of amoxicillin in four tablet brands. *BMC Chem.* **2021**, *15*, 10−11.

(15) Amare, M.; Admassie, S. Potentiodynamic fabrication and characterization of poly (4-amino-3-hydroxynaphthalene sulfonic acid) modified glassy carbon electrode. *J. Mat. Res. Tech.* **2020**, *9*, 11484−11496.
(16) Oztekin, Y.; Yazicigil, Z. Preparation and characterization of a 1, 10-phenanthroline-modified glassy carbon electrode. *Electrochim. Acta* **2009**, *54*, 7294−7298.
(17) Oztekin, Y.; Yazicigil, Z.; Solak, A. O.; Ustundag, Z.; Kilic, Z.; Bilge, S. Surface modification and characterization of phenanthroline nanofilms on carbon substrate. *Surf. Inter. Anal.* **2011**, *43*, 923−930.
(18) Kassa, A.; Abebe, A.; Tamiru, G.; Amare, M. Synthesis of a Novel [diresorcinate-1, 10-phenanthrolinecobalt (II)] Complex, and Potentiodynamic Fabrication of Poly (DHRPCo)/GCE for Selective Square Wave Voltammetric Determination of Procaine Penicillin G in Pharmaceutical and Biological Fluid Samples. *ChemistrySelect* **2022**, *7*, No. e202103458.
(19) Vidya, V. G.; Sadasivan, V.; S Meena, S.; Bhatt, P. Synthesis, spectral and biological studies of complexes with bidentate azodye ligand derived from resorcinol and 1-amino-2-naphthol-4-sulphonic acid. *Orient. J. Chem.* **2018**, *34*, 45−54.
(20) Thakur, U. K.; Shah, D.; Sharma, R. S.; Sawant, R. M.; Ramakumar, K. L. Studies on protonation and Th (IV) complexation behaviour of dihydroxybenzenes in aqueous 1 M NaClO4 medium. *Radiochim. Acta* **2006**, *94*, 859−864.
(21) Jber, N. R.; Abood, R. S.; Al-Dhaief, Y. A. Synthesis and spectral study of new azo-azomethine dyes and its copper (II) complexes derived from resorcinol, 4-aminobenzoylhydrazone and 4-amino antipyrine. *Al-Nah. J. Sci.* **2011**, *14*, 50−56.
(22) Cheraghi, S.; Taher, M.; Karimi-Maleh, H.; Karimi, F.; Shabani-Nooshabadi, M.; Alizadeh, M.; Al-Othman, A.; Erk, N.; Yegya Raman, P. K.; Karaman, C.; Karaman, C. Novel enzymatic graphene oxide based biosensor for the detection of glutathione in biological body fluids. *Chemosphere* **2022**, *287*, 132187.
(23) Kassa, A.; Amare, M.; Benor, A.; Tigineh, G. T.; Beyene, Y.; Tefera, M.; Abebe, A. Potentiodynamic Poly(resorcinol)-Modified Glassy Carbon Electrode as a Voltammetric Sensor for Determining Cephalexin and Cefadroxil Simultaneously in Pharmaceutical Formulation and Biological Fluid Samples. *ACS Omega* **2022**, *7*, 34599−34607.
(24) Baikeli, Y.; Mamat, X.; Wumaer, M.; Muhetaer, M.; Aisa, H. A.; Hu, G. Electrochemical determination of metronidazole using a glassy carbon electrode modified with nanoporous bimetallic carbon derived from a ZnCo-based metal-organic framework. *J. Electrochem. Soc.* **2020**, *167*, 116513−116523.
(25) Sanz, C. G.; Serrano, S. H.; Brett, C. M. Electroanalysis of cefadroxil antibiotic at carbon nanotube/gold nanoparticle modified glassy carbon electrodes. *ChemElectroChem* **2020**, *7*, 2151−2158.
(26) Atif, S.; Baig, J. A.; Afridi, H. I.; Kazi, T. G.; Waris, M. Novel nontoxic electrochemical method for the detection of cefadroxil in pharmaceutical formulations and biological samples. *Microchem. J.* **2020**, *154*, 104574.
(27) Gomaa, E.; Negm, A.; Abou Qurn, R. Cyclic Voltammetry of Cobalt Chloride with L-Carrageenan (LK) Using Glassy Carbon Electrode. *Iran J. Chem. Eng.* **2017**, *14*, 90−99.
(28) Bard, A. J.; Faulkner, L. R. Fundamentals and applications. *Electrochemical Methods* **2001**, *2*, 580−632.
(29) Özer, E.; Sinev, I.; Mingers, A. M.; Araujo, J.; Kropp, T.; Mavrikakis, M.; Mayrhofer, K. J. J.; Cuenya, B. R.; Strasser, P. Ir-Ni bimetallic OER catalysts prepared by controlled Ni electrodeposition on Irpoly and Ir (111). *Surf* **2018**, *1*, 165−186.
(30) Laviron, E. General expression of the linear potential sweep voltammogram in the case of diffusionless electrochemical systems. *J. Electroanal. Chem. Interfac. Electrochem.* **1979**, *101*, 19−28.
(31) Ribeiro, A. R.; Schmidt, T. C. Determination of acid dissociation constants (pKa) of cephalosporin antibiotics: Computational and experimental approaches. *Chemosphere* **2017**, *169*, 524−533.

https://doi.org/10.1021/acsomega.3c00170
ACS Omega 2023, 8, 15181−15192